The Crystal Structure of the AAA Domain of the ATP-Dependent Protease FtsH of *Escherichia coli* at 1.5 Å Resolution

Szymon Krzywda,[1] Andrzej M. Brzozowski,[1,3]
Chandra Verma,[1] Kiyonobu Karata,[2] Teru Ogura,[2]
and Anthony J. Wilkinson[1]
[1]Structural Biology Laboratory
Department of Chemistry
University of York
York YO10 5DD
United Kingdom
[2]Division of Molecular Cell Biology
Institute of Molecular Embryology and Genetics
Kumamoto University
Kumamoto 862-0976
Japan

Summary

Eubacteria and eukaryotic cellular organelles have membrane-bound ATP-dependent proteases, which degrade misassembled membrane protein complexes and play a vital role in membrane quality control. The bacterial protease FtsH also degrades an interesting subset of cytoplasmic regulatory proteins, including σ^{32}, LpxC, and λ CII. The crystal structure of the ATPase module of FtsH has been solved, revealing an α/β nucleotide binding domain connected to a four-helix bundle, similar to the AAA modules of proteins involved in DNA replication and membrane fusion. A sulfate anion in the ATP binding pocket mimics the β-phosphate group of an adenine nucleotide. A hexamer form of FtsH has been modeled, providing insights into possible modes of nucleotide binding and intersubunit catalysis.

Introduction

Intracellular proteolysis is important for eliminating harmful abnormal proteins arising variously through mutational alterations, an imbalance in subunit synthesis in multimeric proteins, or from misfolding or unfolding, as might follow heat shock. It is also important for modulating the activities of authentic proteins, such as short-lived regulatory factors [1]. Intracellular proteolysis in *Escherichia coli* is mediated by a set of five ATP-dependent proteases, Lon, ClpXP, ClpAP, HslUV, and FtsH, which have distinct, as well as overlapping, substrate specificities. FtsH has two special characteristics: it is the only membrane-bound ATP-dependent protease, and it is the only one that is essential for *E. coli* cell growth and viability.

FtsH degrades membrane proteins that have not been appropriately assembled into complexes (Figure 1). Specifically, FtsH has been shown to degrade the unassembled SecY subunit of the protein translocase, the uncomplexed subunit *a* of the F_o sector of the proton ATPase and YccA [2–4]. The rapid degradation of these proteins by FtsH and their highly toxic nature, if accumulated in the cell, point to a key role of FtsH in ensuring the integrity of membrane proteins. An unrelated role in membrane quality control stems from the observation that FtsH specifically degrades LpxC, whose activity is a crucial determinant of the levels of lipopolysaccharide biosynthesis [5]. Degradation of LpxC appears to be the essential function of FtsH, reflecting the importance to the cell of maintaining a balance in the biosynthesis of lipopolysaccharide and phospholipids (Figure 1).

FtsH has a diverse range of other cytoplasmic substrates, which include (1) the heat-shock response RNA polymerase sigma factor, σ^{32} [6], (2) SsrA-tagged proteins [7], and (3) bacteriophage λ proteins CII, CIII, and Xis; therefore, mutations in FtsH lead to a *high frequency* of *lysogeny* phenotype, and FtsH is synonymous with HflB [8–10]. These activities are modulated by the HflK/HflC complex (Figure 1) [4]. Thus, FtsH has a curious dual role in (1) quality control of the cell membrane, guaranteeing appropriate membrane protein assembly and phospholipid balance and (2) governing the stability of intracellular transcription factors that regulate adaptive responses.

The *ftsH* gene in *E. coli* encodes a polypeptide of 647 amino acid residues, and $M_r = 71,000$. It contains two putative transmembrane segments, toward its N terminus, that anchor the protein to the membrane, giving rise to a periplasmic domain of 70 residues and a cytoplasmic domain of 520 residues. The sequence contains a number of motifs, including Walker A (P loop) and B sequences, which point to FtsH's function as an ATPase [11]. There is a further motif, referred to as the SRH (*second region of homology*), whose presence, in combination with the Walker motifs, confers membership of the AAA (*ATPases associated with diverse cellular activities*) family, of which FtsH was the first-identified prokaryotic member. This rather uninformative name reflects the uncertainty of whether these proteins share functional characteristics besides binding and, in most cases, hydrolysis of ATP. The AAA proteins possess sequence similarity over some 240 residues; however, they function in processes as diverse as membrane fusion, organelle biogenesis, transcription regulation, and cell cycle control [12].

Residues 417–421 of FtsH, HEAGH, constitute a Zn^{2+} binding motif characteristic of zinc metalloproteases. Besides this motif, the C-terminal domain has a sequence that is conserved only among FtsH homologs from other bacteria and eukaryotic organelles of endosymbiotic origin, the best characterized being a group of yeast mitochondrial ATPases. FtsH is also highly homologous (41% identity over 500 residues) to a human mitochondrial protein, paraplegin, whose mutation or deletion is linked to hereditary spastic paraplegia [13].

ATP-dependent proteases are complex multisubunit molecular machines. They specifically recognize their
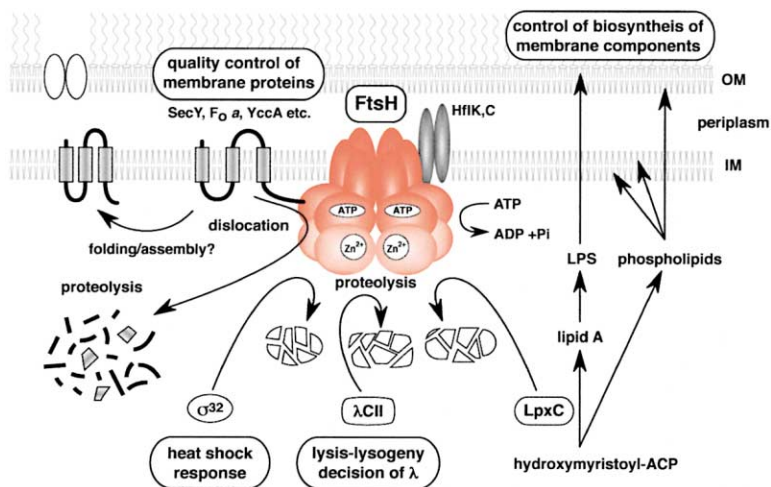
Figure 1. The Cellular Function of FtsH Protease in *E. coli*

FtsH is drawn as a membrane-bound hexameric ring (in red), though its precise oligomeric composition is not known. A subset of its membrane and cytosolic substrates is indicated.

protein substrates and couple ATP hydrolysis to their unfolding and translocation into an interior chamber, where proteolysis takes place. Dramatic insights into their structure and mechanism have emerged from studies of the proteasome, HslUV, and ClpA(X)P [1, 14–19]. HslU, ClpA, and ClpX belong to a larger AAA$^+$ family, of which the AAA proteins are a subfamily, whereas the six regulatory ATPases of the proteasome as well as FtsH belong to the AAA family. With the exception of the strictly defined AAA family, members of the AAA$^+$ family lack the SRH motif [12, 20]. Although ATP-dependent proteases may share a common mechanism of action, there is the additional complexity for FtsH that its membrane protein targets have to be extracted from the lipid bilayer. As a step toward understanding this process, we have determined the crystal structure of the AAA domain of FtsH from *E. coli*. The structure is presented, and comparisons are made with related structures of AAA$^+$ domains.

Results and Discussion

Structure Determination

The AAA domain of *E. coli* FtsH was expressed in a His-tagged form from a pET15b derivative plasmid. Following nickel chelation chromatography, thrombin digestion was expected to produce a polypeptide in which residues 126–398 of FtsH are flanked by three and two residues at the amino and carboxyl termini, respectively. The thrombin digestion products were purified by gel filtration and ion exchange chromatography, and the resulting protein was crystallized from ammonium sulfate solutions [21]. Analysis of the samples used in the crystallization experiments by SDS polyacrylamide gel electrophoresis showed the frequent presence of two protein bands with very similar mobilities. This prompted us to have the amino-terminal sequence of protein from a dissolved crystal determined. Five cycles of Edman degradation revealed an N-terminal sequence, MLTED, corresponding to residues 144–148 of FtsH, leading us to conclude that 18 residues had been trimmed from the expected protein product, presumably through

cleavage after Arg^{143}. As a result, the crystals we have grown are of FtsH(144–398), with a C-terminal Leu-Glu.

The structure was solved by single isomorphous replacement with anomalous scattering using data extending to 2.34 Å spacing collected from a mercury derivative as described in Experimental Procedures. The electron density maps at 1.5 Å resolution are of high quality, allowing almost complete tracing of the polypeptide chain (Figure 2). The refined model contains 251 amino acid residues, five sulfate ions, and 384 water molecules (Table 1). There is no interpretable electron density for residues Gln^{181}–Gly^{185} or for the C-terminal Glu residue, and these residues are assumed to be disordered. The final refined crystallographic R$_{cryst}$ is 0.154 for all data (41,544 reflections) (R$_{free}$ = 0.178) in the resolution range from 50 to 1.5 Å, and the deviations of stereochemical parameters from ideal values are small (Table 1).

Overall Structure

FtsH(144–398) has a two-domain organization, with residues 144–323 forming an α/β domain containing a classical nucleotide binding fold and residues 327–398 forming a four-helix bundle (Figure 3). The core of the nucleotide binding domain is a six-stranded β-pleated sheet, with a strand order β6-β2-β5-β4-β3-β1 and the edge strand β1 running antiparallel to the other five strands (Figure 3A). The β-pleated sheet is flanked by pairs of prominent α helices: α1 and α2 on one surface and α3 and α4 on the other. There is a disruption in the pattern of main chain hydrogen bonding in helix α1, which is noticeably kinked. This may be caused by repulsive interactions among six glutamic acid residues clustered on the exposed surface of this helix. The conserved motifs of the AAA module cluster at the C-terminal end of the strands. The Walker A or P loop motif, which, in FtsH, has the sequence G^{195}PPGTGKT^{202}, connects strand β2 to helix α2 (Figure 3), while the Walker B motif sequence I^{250}IFIDEID^{257} makes up strand β4 and part of the extended loop connecting it to helix α4. The SRH sequence, encompassing residues 299–317, begins toward the end of strand β5 and includes the mean-

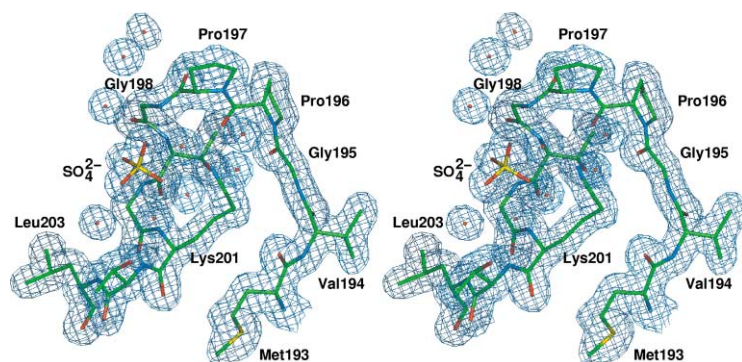Figure 2. Representation of the Final $2F_o - F_c$ Electron Density Maps Contoured at the 1 σ Level in the P Loop Region with the SO_4^{2-} Anion Occupying the Site of the β-Phosphate Group of the Putative ATP Ligand

dering loop that contains two quasi-helical segments that connect $\beta 5$ to $\beta 6$. Two noticeably extended loops connect strand $\beta 3$ to $\alpha 3$ and strand $\beta 4$ to $\alpha 4$.

Comparisons with Other AAA$^+$ Modules

The solution of the crystal structure of the AAA$^+$ module from FtsH brings to eleven the number of such structures, the others being the D2 domain of *N*-ethylmaleimide-sensitive fusion protein from Chinese hamster ovary cells [22, 23], the D1 domain of mouse p97 [24], the ATPase subunit (HslU) of the ATP-dependent protease HslUV from both *E. coli* and *Haemophilus influenzae* [14,

18, 19], an archaeal (*Pyrobaculum aerophilum*) homolog of the prereplication complex protein Cdc6 [25], the Holliday junction migration motor protein RuvB from *Thermus thermophilus* and *Thermotoga maritima* [26, 27], the clamp-loader small subunit RFCS from *Pyrococcus furiosus* [28], the δ, δ′,and γ subunits of the clamp-loader component of *E. coli* DNA polymerase III [29–31], and the ATP binding subunit, BchI, of magnesium chelatase from *Rhodobacter capsulatus* [32]. All are variations on the common structural theme of a RecA-like nucleotide binding fold connected at its C terminus to a structurally less well-conserved helical domain of vari-

Table 1. X-Ray Data and Refinement Statistics

Data Set	Native	MeHgCl
Data Collection and Processing Statistics		
Data collection site	ID14-2 ESRF-Grenoble	14-2 SRS Daresbury
Wavelength (Å)	0.933	1.000
Space group	P4$_1$2$_1$2	P4$_1$2$_1$2
Unit cell dimensions (Å) (a, b, c)	53.15, 53.15, 189.07	53.05, 53.05, 188.12
Resolution range (Å) (outer shell)	50–1.5 (1.55–1.50)	40–2.34 (2.39–2.34)
Observations	913,258	85,309
Unique reflections	44,655	14,527
Completeness (%)	98.4 (91.1)	87.7 (78.9)
I/σ(I)	18.3 (2.6)	24.9 (7.7)
R$_{merge}$[a]	0.064 (0.261)	0.041 (0.099)
Phasing power[b] (acentric/centric)		1.41/1.13
R$_{cullis}$ (isomorphous/anomalous)[c]		0.68/0.79
Figure of merit[d] (MLPHARE[c,a]/DM[com])		0.43[c], 0.56[a]/0.65[com]
Refinement Statistics		
Resolution range (Å)	50–1.5	
Reflections used (R$_{free}$ set)	421,544 (2,198)	
R$_{cryst}$ (R$_{free}$)[e]	15.4 (17.8)	
Protein/waters/ions atoms	1,977/384/25	
Rms bonds/angles[f]	0.018 Å/1.811°	
Rms main chain ΔB (Å^2)[g]	1.339	
Mean B factor (Å^2)[h]	28.1/25.4/28.5/33.7/36.2	
Percentage of A, B, and L (a, b, l, p)[i]	93.3 (6.7)	

[a] R$_{merge}$ = 100 × Σ|I − <I>|/Σ<I> (for all data—no sigma cutoff).
[b] Phasing power = rms (|F$_h$|/E), where |F$_h$| is the heavy atom structure factor amplitude and E is the is the residual lack of closure.
[c] R$_{cullis}$ = rmsf/E$_{iso}$ (root-mean-square heavy atom F/isomorphous lack of closure error [phasing power]).
[d] Figure of merit = weighted mean of the cosine of the deviation from α$_{best}$ (after MLPHARE and DM) (for c, centric; a, acentric data; com, combined).
[e] R$_{cryst}$ = Σ|F$_{obs}$ − F$_{calc}$|/ΣF$_{obs}$; R$_{free}$ is as R$_{cryst}$ but is calculated over 5% of data that were excluded from the refinement process.
[f] Root-mean-square deviations in bond length and angle distances from Engh and Huber ideal values.
[g] Root-mean-square deviations between B factors for bonded main chain atoms.
[h] Mean temperature factor for the whole molecule (including solvent), main chain, side chain, water, and ligand (sulphate) atoms, respectively.
[i] Percentage of residues located in the most-favored (additional) regions of Ramachandran plot, as determined by PROCHECK [49].
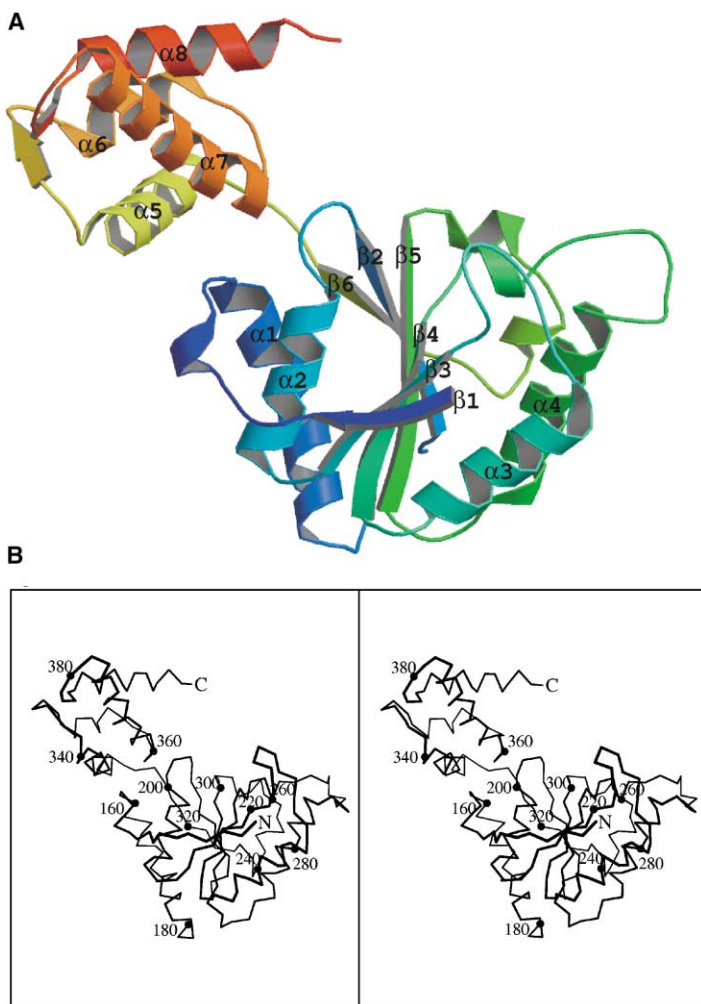
A

B

Figure 3. The Overall Fold of FtsH(144–398)

(A) Ribbon tracing. The chain is color ramped from blue at the amino terminus (residue 144) to red at the carboxyl terminus (residue 398). The prominent β strands and α helices are labeled.

(B) Stereo C_α trace with the N and C termini and every 20th residue labeled. These figures were drawn in the program MOLSCRIPT [53].

able size. A total of 120–140 residues from the RecA-like domains of the respective proteins can be superposed onto that of FtsH(144–398), with a root-mean-square deviation (rmsd) in equivalent C_α positions of 1.7–3.2 Å [33].

The most obvious difference between FtsH and the other AAA$^+$ domain proteins is the extension of the common five-stranded parallel β sheet to six strands, as a consequence of the packing of residues 145–149 in an antiparallel fashion against the edge of the sheet. The δ subunit of the clamp-loader complex also has a sixth amino-terminal strand to its β sheet; however, in this case, the extra strand runs parallel to, and is attached to the opposite edge of, the sheet [30]. The AAA domain of FtsH has closest similarity in sequence to the ATPase domains of the membrane fusion factors p97 and NSF. As shown in Figure 4A, after overlapping the C_α atoms of the P loop residues by least-squares minimization procedures, these three molecules superimpose closely. The close superimposition extends across the interdomain linker into the helical domain. This is impressive, given that three different liganded forms, unliganded (FtsH), ADP bound (p97-D1), and ATP bound (NSF-D2), are being compared. The structures are divergent at the N terminus, where NSF-D2 and FtsH(144–398) have been artificially truncated. In FtsH(144–398), the N-ter-

minal segment would lead back to a transmembrane segment, whereas, in the NSF-D2 and p97-N-D1 structures, the adjacent sequences are involved in binding the adenine base of the nucleotide and in connecting to the D1 and N domains, respectively. The second region of obvious structural divergence is in the extended segment corresponding to the β4-α4 loop of FtsH (Figure 4A). The conformation of this loop is quite different in all three structures. The presence of five glycines in a string of seven residues suggests that this loop is intrinsically flexible in FtsH. In the crystal, its conformation is strongly influenced by intermolecular contacts, as described below.

A search for structural similarity to the C-terminal helical domain in the program DALI [33] also picked up corresponding domains from a series of AAA$^+$ family members, by far the closest similarity being with p97 [24], where 68 of 71 residues can be overlapped with an rmsd in C_α atom positions of 0.7 Å. An interesting high-scoring exception is the histone protein HMk from *Methanopyrus kandleri*, where 70 residues can be overlaid with an rmsd in C_α atom positions of 2.8 Å [34].

Ligand Binding Site

The ligand binding pocket in FtsH(144–398) does not contain nucleotide, consistent with the observation that
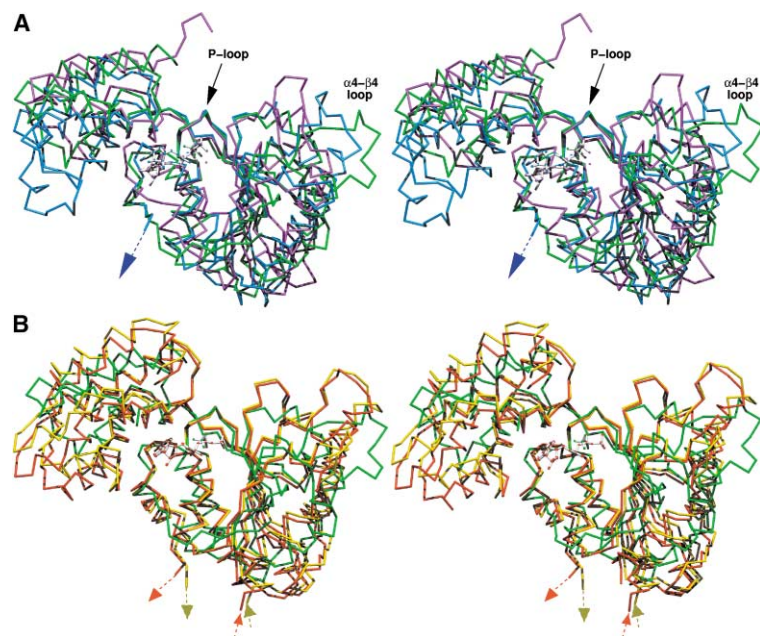
Figure 4. Comparison of the Structures of the AAA Modules of FtsH, p97-D1, NSF-D2, and HslU

(A) Stereo backbone trace of the AAA module of FtsH (green) overlaid onto the structures NSF-D2 (magenta) and p97-D1 (blue).

(B) Overlap of FtsH(144–398) (green) onto unliganded (yellow) and Mg-ATP-liganded (red) HslU. The ligands are shown as ball and stick models. The structures have been superimposed by least-squares minimization of the positions of the C$_\alpha$ atoms of the P loop residues. The arrows indicate links with additional, more-specific domains, omitted here for picture clarity.

the same crystal form was obtained in the presence and absence of ATP or AMPPNP in the crystallization solution. A prominent tetrahedral feature in the electron density maps (Figure 2) in the vicinity of the P loop has been modeled as a sulfate ion that was presumably introduced into the molecule through the crystallization solutions in which $(NH_4)_2SO_4$ was used as a precipitant. Upon refinement, the atoms of the sulfate exhibit temperature factors similar to those of surrounding protein atoms. The divalent anion forms charge-dipole interactions with main chain amide N-H groups of the P loop residues Gly^{198}, Gly^{200}, and Lys^{201} as well as an ion-pairing interaction with the side chain of Lys^{201} (Figure 5A). The latter pair of interactions is reminiscent of the interactions formed by the oxygens of the β-phosphate groups of nucleotides bound to other P loop ATPases (Figure 5B). The ε-amino group of the P loop lysine forms an additional interaction with the γ-phosphate group of nucleotide triphosphate ligands in other AAA$^+$ proteins. Consistent with its anticipated role in nucleotide binding in FtsH, the substitution of Lys^{201} by site-directed mutagenesis leads to loss of activity [35].

The sulfate anion forms additional polar interactions with the P loop residues mediated by four water molecules, which themselves contribute to a well-ordered solvent network. One of these waters forms a hydrogen bond with the hydroxyl of Thr^{202}. In NSF-D2 complexed with AMPPNP, the corresponding threonine hydroxyl is bonded to a magnesium ion that coordinates oxygen atoms from the β- and γ-phosphates in addition to three water molecules [22].

In the crystal structures of other AAA$^+$ domain proteins, adenine nucleotides are invariably present, featuring ATP, AMPPNP, ADP, and dADP. Exceptions are the BchI component of the magnesium chelatase, the *E. coli* clamp loader's δ′ and δ subunits, which do not bind to ATP, and two crystal forms of HslU. In an orthorhombic HslU crystal form solved to 3.0 Å resolution, only four of the six subunits of the hexamer contain nucleo-

tide [14]. In the remaining pair of subunits, situated opposite each other in the hexamer, ATP is absent, and a sulfate ion is enclosed in the P loop. After overlapping the P loop elements of these HslU subunits onto that of FtsH(144–398), the sulfur atoms in the respective structures are displaced by only 0.4 Å (Figure 5B).

Mutagenesis Correlations

Sequence comparisons led to the identification of the SRH (*second region of homology*) as a conserved motif of 19 or so residues that distinguishes the AAA family from the larger superfamily of Walker-type ATPases. More extensive sequence and structural comparisons have led to the definition of a AAA$^+$ family that embraces the AAA subfamily and includes, in addition, proteins that share the AAA fold, but lack the SRH. An alanine-scanning mutagenesis study of the SRH of FtsH, encompassing residues 299–317, has confirmed the importance of this motif for FtsH function. Asn^{301}, Asp^{307}, Arg^{312}, and Arg^{315} were shown to be essential for activity, with mutations of Thr^{300}, Arg^{302}, Leu^{306}, and Leu^{310} having measurable, but less severe, effects on the in vivo degradation of a σ^{32} substrate [35, 36].

In an attempt to account for the functional effects of the mutations in structural terms, we built a homology model of the FtsH AAA domain based on the crystal structure of the hexamerization domain of NSF-D2 [36]. In the modeled FtsH-AAA, the bound nucleotide formed a multitude of contacts with surrounding residues, including canonical interactions between the Mg^{2+} and β- and γ-phosphate moieties and residues of the Walker A and B motifs. The modeled SRH contains a short α helix flanked by extended segments. Residues Asn^{301} and Arg^{315} were located in hydrogen bonding distance of the γ-phosphate of ATP, though, in the case of Arg^{315}, the interaction is with the ATP in a neighboring subunit. As a result, Asn^{301} and Arg^{315} were assigned possible roles as phosphate-group sensors. The side chains of Arg^{312} and Asp^{307} formed a bidentate salt-bridging inter-
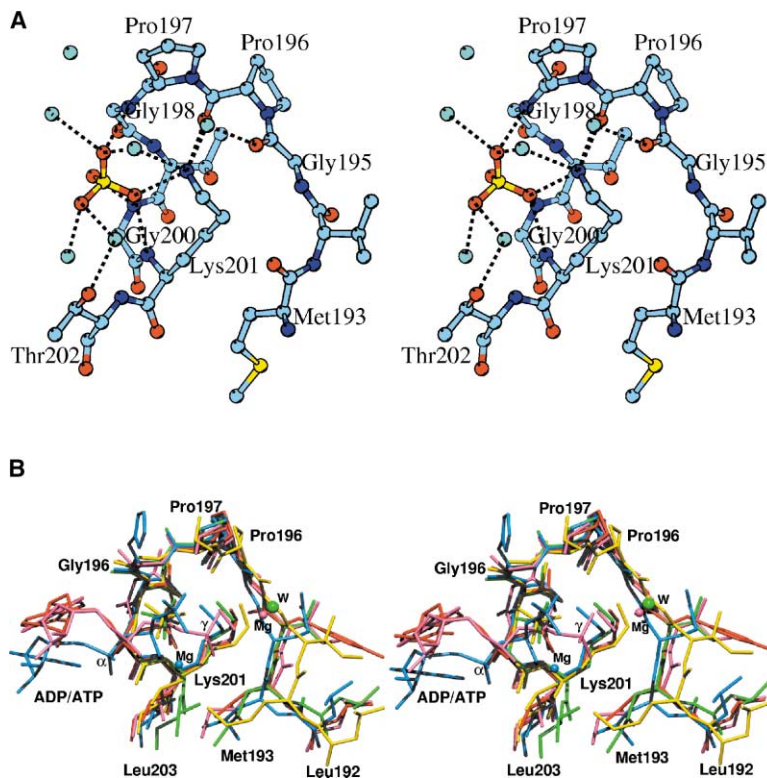
Figure 5. The P Loop Pocket of FtsH

(A) Stereo view of the interactions of the sulfate ion and the P loop residues. Atoms are colored according to type: carbon, light blue; oxygen, red; nitrogen, dark blue; sulfur, yellow; water molecules, cyan. Hydrogen bonding/electrostatic interactions are indicated by dashed lines.

(B) Comparison of sulfate binding in the P loop pockets of FtsH(144–398) (green) and HslU (yellow) with nucleotide binding in p97-D1 (red), NSF-D2 (blue), and HslU (pink). The anions and nucleotides were superposed by least-squares minimization of differences in positions of the eight C_α atoms of the P loop residues in the respective proteins.

action, though it was not clear why such an interaction would be essential.

Comparison of the homology model with the experimentally determined structure presented here is complicated by the absence of nucleotide in the latter and the finding that FtsH(144–398) is not a hexamer. In the crystal structure, the main chain of the SRH meanders across the side of the α/β domain, its course constrained by three proline residues, 303, 308, and 313. Asn[301] and Arg[315] project out into the solvent, though both are well defined. The latter side chain lies parallel to that of Arg[312]. A pair of sulfates (2 and 3) is associated with the SRH. Sulfate 2 makes a charge-dipole interaction with Asn[301] and a two-pronged salt-bridging interaction with Arg[302], while a pair of oxygens from sulfate 3 makes ion-pairing interactions with $N_\epsilon H$ and $N_\zeta H_2$ of Arg[312]. In contrast to the model, Asp[307] does not participate in a salt linkage to Arg[312] and instead points into the solvent, while Arg[315] forms a tight salt linkage to Asp[286].

Intersubunit Interactions

Examination of the packing of FtsH(144–398) in the crystal reveals the presence of a very compact dimer. The surface area buried as a result of dimer formation is 1502 Å². As shown in Figure 6, two molecules related by the 2-fold crystallographic symmetry axis come together, forming an extensive set of intermolecular interactions. In particular, residues 145–149 from each partner molecule align in an antiparallel fashion at the center of the dimer to form β sheet interactions. As a result, the six-stranded sheets in each monomer are extended into a twelve-stranded intermolecular β sheet in the dimer (Figure 6). In addition, helices α7 from each subunit

form extensive interacting surfaces with loops β3-α3 and β4-α4 of the partner subunit. Asp[223] and Phe[224] close off the adenine-ribose pocket of the partner molecule in the dimer, accounting for our inability to successfully soak nucleotide ligands into the crystal.

Structures of AAA$^+$ domains crystallized either as isolated fragments or in their intact proteins have revealed the presence of hexameric rings in NSF-D2, p97-D1, and HslU, a distorted hexamer in RFCS, a heteropentamer in the case of the $\delta'\gamma_3\delta$ DNA polymerase clamp-loader complex, and monomers in BchI, RuvB, Cdc6, and the isolated δ' subunit of DNA polymerase. Dimers are therefore without precedent. The prevailing opinion is that AAA proteins function as homo- or heterooligomers of five to seven, but most commonly six, subunits. Ring-shaped oligomers of FtsH have been observed by electron microscopy, though the images were not of sufficient resolution to allow definition of the number of subunits involved [8].

The absence of a hexamer structure for FtsH(144–398) is not entirely unexpected, as studies of Akiyama and Ito (2000) [37] have suggested that the most significant determinants of FtsH oligomerization reside in the transmembrane and periplasmic portion of the molecule. Deletion of the N-terminal 123 residues from FtsH to give FtsH(ΔTM) leads to loss of activity against both membrane-bound and cytoplasmic substrates and an inability to form homooligomers; FtsH(ΔTM) is a monomer [37]. Interestingly, the fusion of FtsH(ΔTM) to the leucine zipper element from GCN4, which generates a dimer in vitro, restores activity toward cytoplasmic, but not membrane-bound, substrates, whereas fusion of FtsH(ΔTM) to the first and second transmembrane elements of LacY restores activity against both sets of substrates.
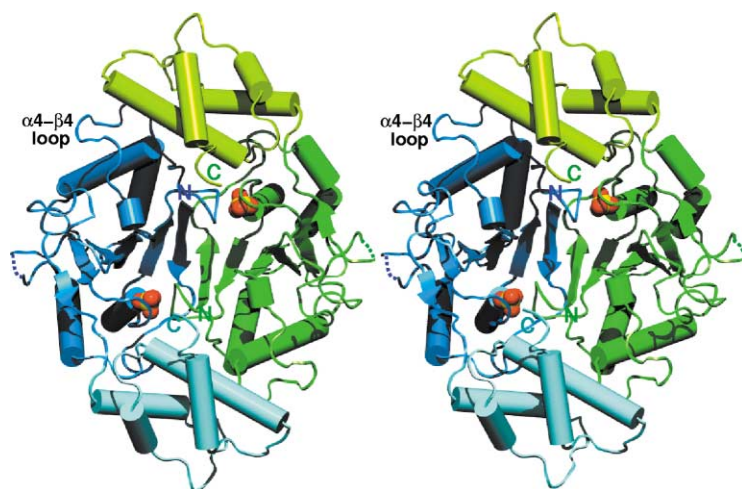
Figure 6. An FtsH(144–398) Crystallographic Dimer

Two FtsH(144–398) protomers related by a crystallographic 2-fold symmetry operation are depicted. The domains of one protomer are colored different shades of blue; those of the other protomers are colored different shades of green. The 12-stranded β-pleated sheet running across the center of the dimer from left to right is apparent. The sulfate anion bound in the ATP binding pocket is depicted by red and yellow van der Waals spheres. The termini (N and C) of the protein and the α4-β4 loop are labeled. Residues 181–185, which are missing from the model, are indicated as a dotted line.

The significance, if any, of the FtsH(144–398) dimer observed here is not established. Its precursor, FtsH(126–398) exhibits characteristics of a monomer in gel filtration and in dynamic light-scattering experiments. It seems likely, therefore, that the dimer arises from the further truncation of 18 residues distal to the second transmembrane segment that allows residues 145–149 to pack onto the edge of the β sheet and mediate dimer formation. These considerations and the occlusion of the nucleotide binding site by the close packing of residues from the partner subunit (especially of the 222–228 loop) argue that this dimer is not physiologically relevant.

Modeling and Mechanism
We have built a model of an FtsH(144–398) hexamer, guided by the arrangement of the subunits in the 6-fold symmetric NSF-D2 assembly [22, 23]. NSF-D2 was preferred as a template for molecular modeling because it shares sequence similarity with FtsH and its structure has been solved to high resolution. To achieve satisfactory packing, we needed to alter the conformation of the β4-α4 loop, which otherwise forms significant intermolecular clashes (Figure 7A). The packing in the hexamer is somewhat looser in the FtsH model than it is in NSF-D2, which may reflect the fact that the latter is the hexamerization domain of intact NSF fusion protein, whereas, in FtsH, oligomerization is mediated by the transmembrane/periplasmic domain.

In the model, the C termini of the six chains are situated on what we will call the assembly's C surface, which is the front-facing surface in Figure 7A, whereas the N termini are situated on the opposite face, the N surface. Viewed from the C-terminal side, the β3-α3 loops that form a prominent surface of the central hole point in a clockwise direction, instead of in the anticlockwise arrangement in our previous homology model (Figure 7A) [36].

Mg-ATP can be accommodated in the intermolecular pockets of the modeled unliganded hexamer, with only minor alterations in protein side chain conformations.

The environment of the bound ATP is illustrated in Figure 8. Lys^{201} makes hydrogen bonds to the β- and γ-phosphate oxygens. The carboxylate of Asp^{254} of the Walker B motif forms a hydrogen bond with a water molecule, which is liganded to the Mg^{2+} ion that additionally coordinates the β- and γ-phosphate oxygens and the hydroxyl of Thr^{202}. The neighboring Glu^{255} carboxylate is well placed to activate a water molecule for in-line attack at the γ-phosphorus. The amide group of Asn^{301} of the SRH is appropriately positioned to act as a γ-phosphate-group sensor, possibly through the mediation of a water molecule. The charged side chain of Arg^{312} makes an ion-pairing contact with the γ-phosphate of the nucleotide in the neighboring subunit. As suggested by Zhang et al. [24], this residue appears more likely than Arg^{315} to serve as an arginine finger. In addition, the ATP is stabilized by several hydrogen bonds to the backbone, both directly and through water molecules.

The locations of the AAA chain termini in the model are most easily reconciled with the N surface being apposed to the cytoplasmic membrane and the C surface facing the peptidase domain. Crystallographic observations on HslU and proteolytic and electron microscopic analyses of ClpA and ClpX show that a topologically equivalent surface contacts the protease subunits in these systems [19, 38]. An electrostatic potential energy surface for the FtsH(144–398) hexamer has been calculated and is shown in Figures 7B–7D. Neither face of the hexamer exhibits any significant polarization in the charge distribution. In view of the expected proximity of the AAA domain to the negatively charged phospholipid bilayer, this is perhaps surprising. The perimeter of the disk is more basic in character, which might imply a more sideways orientation of the cytoplasmic domains of FtsH with respect to the membrane than is implied by Figure 1. The central hole is clearly acidic in character, when viewed from the N-terminal side, as a result of the clustering of the Asp^{272} and Glu^{273} side chains that line its surface. Passing through the lumen, these acidic residues are flanked on the N-terminal face by residues $M^{227}FVG^{230}$ corresponding to the pore 1 motif defined by Wang et al. [19] and on the C-terminal face by residues $G^{264}AGLGGGH^{271}$ overlapping with the sequence corre-
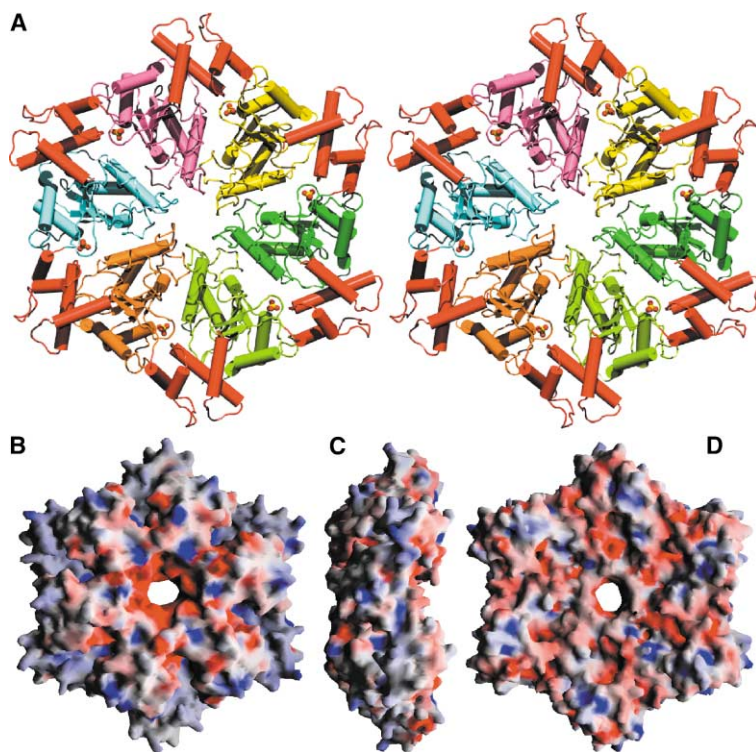
Figure 7. Modeling of an FtsH(144–398) Hexamer

(A) Stereo view of a modeled FtsH hexamer. The α/β domain of each protomer is colored differently, while the C-terminal α domains are in red.

(B–D) Electrostatic surfaces calculated in the program GRASP [54] on the ligand-free hexamer of FtsH(144–398) and displayed on the C-terminal face (B), the side (C), and the N-terminal face (D). The potentials are colored from −10 kT (red) to +10 kT (blue).

sponding to the pore 2 segment in HslU [19]. It has been proposed that the Tyr[91] residues in HslU hexamers play an important role in unfolding coupled translocation, and the corresponding Phe[228] residues in the FtsH model are well placed to play a similar role.

The specificity that AAA$^+$ proteases exhibit toward their substrates is imposed by the ATPase modules. This has been clearly illustrated for the bacterial cytoplasmic enzymes, where the C-terminal α-helical domains are referred to as sensor and substrate discrimination domains [39]. In the modeled hexamer these have a peripheral location and are slightly displaced to the C surface of the ring. Again by analogy with the Clp systems, it is expected that the unfolding substrate polypeptide will be threaded through the hole in the AAA ring from the

N-terminal face, which is expected to be membrane proximal to the C-terminal membrane-distal side, where the protease compartment is expected to be located [16, 17]. It has been shown that proteolysis of YccA and SecY derivatives by FtsH proceeds from the substrate's N terminus [40]. The negative potential surrounding the hole in the AAA module may facilitate the initial approach of the substrate. Threading trajectories for a model tetrapeptide showed that an N-terminal approach of the ligand was energetically more favorable than a C-terminal approach [36] (http://www.ysbl.york.ac.uk/~chandra/AAA). To test the validity of basing the modeling on the NSF-D2 hexamer, we also constructed models for the FtsH hexamer using p97 and HslU as templates [19, 24]. In these systems the orientation of the α/β domains
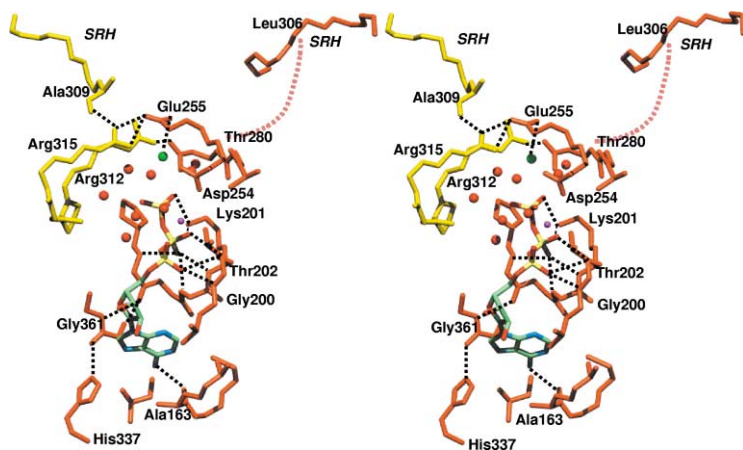

Figure 8. Proposed ATP Binding Mode in the Modeled Hexamer

Adjacent protein subunits are colored in yellow and orange, with the ATP atoms colored according to element. Waters are represented as red spheres, with the exception of the "activated" water, which is in green; the Mg^{2+} cation is represented as a magenta sphere. For clarity, only the most relevant hydrogen bonds (in black dashed lines) are shown. The orange dashed line indicates a route by which chemical changes at the γ-phosphate may be propagated through Glu[255] and the SRH to the ATP bound to the neighboring subunit.

differ; however, the key interactions with the nucleotide are preserved, and the global electrostatic potentials are qualitatively similar.

Biological Implications

E. coli FtsH is an essential membrane-bound ATP-dependent zinc metalloprotease. Enzymes with a high degree of sequence similarity to FtsH are found in the organelles of eukaryotic cells, and one of these homologs, paraplegin, is associated with human disease. FtsH plays a curious dual role in membrane quality control. First, it helps to maintain a balance in the lipid composition of the membrane by degrading LpxC, the regulatory enzyme in the pathway of lipid A biosynthesis. Second, FtsH is responsible for degrading misassembled membrane proteins. In carrying out this reaction, FtsH's membrane protein substrates appear to be extracted from the membrane in an ATP-dependent reaction. By analogy with the soluble ATP-dependent proteases, FtsH is expected to form an oligomeric ring-shaped assembly in which ATP hydrolysis is coupled to substrate unfolding and translocation into an enclosed proteolytic cavity. To address the structural basis of membrane protein degradation, we have solved the crystal structure of the central ATPase domain of FtsH that connects the transmembrane/periplasmic domain at the N terminus to the proteolytic domain at the C terminus. The structure is remarkably similar to the chemomechanical converter components or AAA modules of a number of proteins that have diverse cellular functions. The structure reveals an unliganded monomer. A sulfate ion in the adenine nucleotide binding pocket and structural comparisons point to a mode of ATP binding, allowing putative protein nucleotide interactions to be identified. A hexamer of the FtsH ATPase has been constructed by homology modeling. The model accounts for the functions of many protein residues that have been shown by mutagenesis to be essential for function, in particular, residues in the so-called second region of homology (SRH), which function as γ-phosphate-group sensors within and between subunits. The solution of the structure of the ATPase domain of FtsH will facilitate studies of the intact protein, leading to a fuller understanding of the function of this remarkable molecular machine.

Experimental Procedures

X-Ray Diffraction Data Collection and Reduction

Tetragonal crystals of the 144–398 fragment of FtsH were grown from 0.1 M Tris-HCl (pH 8.5) and 1.5 M $(NH_4)_2SO_4$ as described [21]. Diffraction data from native crystals extending to 1.5 Å resolution were collected at station ID14-2 ($\lambda = 0.933$ Å) at ESRF-Grenoble (Table 1) on an ADSC CCD detector in three sweeps. Molecular replacement calculations employing different programs and using a number of available AAA$^+$ coordinate sets as search models did not produce a satisfactory solution. Isomorphous replacement strategies were therefore explored. An FtsH crystal was soaked for 2 hr in a mother liquor solution containing 5 mM methyl mercury chloride (MeHgCl). The soaked crystal was subsequently scooped through a cryoprotectant solution (mother liquor supplemented with 25% glycerol and 5mM MeHgCl) and flash-cooled in liquid N_2. A 2.3 Å resolution single anomalous dispersion (SAD) diffraction data set

was collected from this crystal at 100 K on station 14-2 at the SRS Daresbury ($\lambda = 1.000$ Å). Six hundred images were recorded on an ADSC CCD detector using an oscillation angle of 0.25° and an exposure time of 5 s. Native and heavy atom derivative data processing were carried out with the programs DENZO and SCALE-PACK [41].

SIRAS Phasing

Isomorphous and anomalous difference Patterson maps showed clear peaks, consistent with a single heavy atom substitution. Version 2.02 of the program SOLVE [42] was used to locate a single mercury site. Further refinement of this heavy atom position in MLPHARE [43], using both the isomorphous and the anomalous difference terms, yielded phases with an overall figure of merit (FOM) of 0.43 and a phasing power of 1.41. Although the derivative data are effectively complete (97%) only as far as 2.5 Å spacing, additional reflections extending to 2.34 Å spacing (78% completeness in 2.39–2.34 Å resolution bin) were used in heavy atom refinement. Initial phases calculated in MLPHARE were improved and extended to 1.5 Å spacing with the native data set by histogram matching, multiresolution density modification, and solvent flattening (using a solvent content of 0.45) with the program DM [44], yielding a final FOM of 0.65 for all data to 1.5 Å spacing and 0.81 for data to 2.0 Å resolution.

Model Building and Refinement

The final DM electron density maps were of excellent quality, allowing application of automatic model building using the warpN-trace routines in the program ARP [45], which produced a model consisting of five chain segments and 228 of the expected 256 residues, with a connectivity of 0.96 and an R_{cryst} of 0.198. Cycles of manual corrections to the model, building of missing loops, and location of the water molecules during the refinement process were performed with the X-AUTOFIT and X-SOLVATE routines of the molecular graphics package QUANTA (QUANTA98; Accelrys, San Diego, CA). Initial TLS and isotropic temperature factor refinement in REFMAC [46, 47], with the use of all the X-ray terms, were followed by an anisotropic refinement in the same program, converging with a crystallographic R_{cryst} of 0.154 and an R_{free} of 0.178. All data manipulation, phasing (except SOLVE), and refinement were carried out using Version 4.1.1 of the CCP4 suite of programs (CCP4, 1994) [48], as implemented in the CCP4Interface version 4.1.1.

The final FtsH model consists of 1977 protein atoms, 384 waters, and 5 sulfate ions (Table 1). It spans from Met^{144} to Gly^{398} of FtsH, with an additional C-terminal Leu, the only gap in the chain occurring from residues 180 to 185, for which there is no electron density, and these residues are assumed to be disordered. An analysis of the model's stereochemistry in PROCHECK [49] reveals that 93.3 % of the residues are in most-favored regions of the Ramachandran plot, with the remaining 6.7 % of residues in the additionally allowed regions. The crystallographic dimer discussed here can be generated from the monomer atomic coordinates by application of the −y, −x, and 1/2 − z rotational and (1 1 0) translational symmetry operations.

Molecular Modeling

The CHARMM-19 polar hydrogen force field [50] was used for all calculations, and the parameters used were as described in Karata et al. [36]. Hydrogen atoms were added to the crystal structure of FtsH(144–6398) using the HBUILD functionality [51] of CHARMM. The orientations of Asn/Gln side chains and the appropriate protonations of the His residues were subsequently optimized [52]. The SO_4^{2-} molecule that was located within the P loop was retained. The monomer was subjected to rounds of energy minimizations (using combinations of steepest descent and adopted basis Newton-Raphson algorithms [50] to alleviate the effects of crystal contacts). The monomer was then superposed onto the backbone of six NSF-D2 monomers generated using the symmetry operators and the coordinate set 1d2n [22]. It was immediately apparent that residues Val^{225}-Glu^{226}-Met^{227} of the β3-α3 loop were clashing with the neighboring subunit. Guided by the conformation of this loop in our earlier model [36], we manually manipulated the extended

region Phe^{224}–Phe^{228} and then minimized the energy. The minimization enabled residues 224–228 to relax, while surrounding atoms were subject to tight restraints. The ensuing conformational changes, whose associated barriers are easily traversable at room temperatures [52], removed the clashes. The hexamer was reconstructed, solvated, and subjected to rounds of restrained refinement using a combination of energy minimizations and molecular dynamics simulations [36].

In order to examine the structural differences that might accompany nucleotide binding, Mg-ATP was built into the binding site situated between one pair of monomers in the hexamer. The ligand geometry was optimized by energy minimization of the Mg-ATP and protein residues within 6 Å, while the rest of the hexamer was held fixed. A fully Mg-ATP-liganded hexamer was then generated by applying symmetry operations and energy minimization procedures as described above. All figures, except Figures 1, 3, and 5A, were made in QUANTA.

References

1. Schmidt, M., Lupas, A.N., and Finley, D. (1999). Structure and mechanism of ATP-dependent proteases. Curr. Opin. Chem. Biol. *3*, 584–591.
2. Kihara, A., Akiyama, Y., and Ito, K. (1995). FtsH is required for proteolytic elimination of uncomplexed forms of SecY, an essential protein translocase subunit. Proc. Natl. Acad. Sci. USA *92*, 4532–4536.
3. Kihara, A., Akiyama, Y., and Ito, K. (1998). Different pathways for protein degradation by the FtsH/HflKC membrane-embedded protease complex: an implication from the interference by a mutant form of a new substrate protein, YccA. J. Mol. Biol. *279*, 175–188.
4. Akiyama, Y., Kihara, A., and Ito, K. (1996). Subunit *a* of proton ATPase F$_0$ sector is a substrate of the FtsH protease in Escherichia coli. FEBS Lett. *399*, 26–28.
5. Ogura, T., Inoue, K., Tatsuta, T., Suzaki, T., Karata, K., Young, K., Su, L.-H., Fierke, C.A., Jackman, J.E., Raetz, C.R.H., et al. (1999). Balanced biosynthesis of major membrane components through a regulated degradation of the committed enzyme of lipid A biosynthesis by the AAA protease FtsH (HflB) in Escherichia coli. Mol. Microbiol. *31*, 833–844.
6. Tomoyasu, T., Gamer, J., Bukau, B., Kanemori, M., Mori, H., Rutman, A.J., Oppenheim, A.B., Yura, T., Yamanaka, K., Niki, H., et al. (1995). *Escherichia coli* FtsH is a membrane-bound, ATP-dependent protease which degrades the heat-shock transcription factor σ^{32}. EMBO J. *14*, 2551–2560.
7. Herman, C., Thévenet, D., Bouloc, P., Walker, G.C., and D'Ari, R. (1998). Degradation of carboxy-terminal-tagged cytoplasmic proteins by the *Escherichia coli* protease HflB (FtsH). Genes Dev. *12*, 1348–1355.
8. Shotland, Y., Koby, S., Teff, D., Mansur, N., Oren, D.A., Tatematsu, K., Tomoyasu, T., Kessel, M., Bukau, B., Ogura, T., et al. (1997). Proteolysis of the phage λ CII regulatory protein by FtsH (HflB) of *Escherichia coli*. Mol. Microbiol. *24*, 1303–1310.
9. Herman, C., Thévenet, D., D'Ari, R., and Bouloc, P. (1997). The HflB protease of *Escherichia coli* degrades its inhibitor λ cIII. J. Bacteriol. *179*, 358–363.
10. Leffers, G.G., Jr., and Gottesman, S. (1998). Lambda Xis degradation in vivo by Lon and FtsH. J. Bacteriol. *180*, 1573–1577.
11. Walker, J.E., Saraste, M., Runswick, M.J., and Gay, N.J. (1982).

12. Distantly related sequences in the α- and β-subunits of ATP synthase, myosin, kinases and other ATP-requiring enzymes and a common nucleotide binding fold. EMBO J. *1*, 945–951.
12. Ogura, T., and Wilkinson, A.J. (2001). AAA$^+$ superfamily ATPases: common structure-diverse function. Genes Cells *6*, 575–597.
13. Casari, G., De Fusco, M., Ciarmatori, S., Zeviani, M., Mora, M., Fernandez, P., De Michele, G., Filla, A., Cocozza, S., Marconi, R., et al. (1998). Spastic paraplegia and OXPHOS impairment caused by mutations in paraplegin, a nuclear-encoded mitochondrial metalloprotease. Cell *93*, 973–983.
14. Bochtler, M., Hartmann, C., Song, H.K., Bourenkov, G.P., Bartunik, H.D., and Huber, R. (2000). The structures of HslU and the ATP-dependent protease HslU-HslV. Nature *403*, 800–805.
15. Ishikawa, T., Maurizi, M.R., Belnap, D., and Steven, A. (2000). Docking of components in a bacterial complex. Nature *408*, 667–668.
16. Ishikawa, T., Beuron, F., Kessel, M., Wickner, S., Maurizi, M.R., and Steven, A.C. (2001). Translocation pathway of protein substrates in ClpAP protease. Proc. Natl. Acad. Sci. USA *98*, 4328–4333.
17. Ortega, J., Singh, S.K., Ishikawa, T., Maurizi, M.R., and Steven, A.C. (2000). Visualization of substrate binding and translocation by the ATP-dependent protease, ClpXP. Mol. Cell *6*, 1515–1521.
18. Sousa, M.C., Trame, C.B., Tsuruta, H., Wilbanks, S.M., Reddy, V.S., and McKay, D.B. (2000). Crystal and solution structures of an HslUV protease-chaperone complex. Cell *103*, 633–643.
19. Wang, J., Song, J.J., Franklin, M.C., Kamtekar, S., Im, Y.J., Rho, S.H., Seong, I.S., Lee, C.S., Chung, C.H., and Eom, S.H. (2001). Crystal structures of the HslVU peptidase-ATPase complex reveal an ATP-dependent proteolysis mechanism. Structure *9*, 177–184.
20. Neuwald, A.F., Aravind, L., Spouge, J.L., and Koonin, E.V. (1999). AAA$^+$: a class of chaperone-like ATPases associated with the assembly, operation, and disassembly of protein complexes. Genome Res. *9*, 27–43.
21. Krzywda, S., Brzozowski, A.M., Karata, K., Ogura, T., and Wilkinson, A.J. (2002). Crystallization of the AAA domain of the ATP-dependent protease FtsH of *Escherichia coli*. Acta Crystallogr. D Biol. Crystallogr. *58*, 1066–1067.
22. Lenzen, C.U., Steinmann, D., Whiteheart, S.W., and Weis, W.I. (1998). Crystal structure of the hexamerization domain of N-ethylmaleimide-sensitive fusion protein. Cell *94*, 525–536.
23. Yu, R.C., Hanson, P.I., Jahn, R., and Brunger, A.T. (1998). Structure of the ATP-dependent oligomerization domain of N-ethylmaleimide sensitive factor complexed with ATP. Nat. Struct. Biol. *5*, 803–811.
24. Zhang, Y., Shaw, A., Bates, P.A., Newman, R.H., Gowen, B., Orlova, E., Gorman, M.A., Kondo, H., Dokurno, P., Lally, J., et al. (2000). Structure of the AAA ATPase p97. Mol. Cell *6*, 1473–1484.
25. Liu, J., Smith, C.L., DeRyckere, D., DeAngelis, K., Martin, G.S., and Berger, J.M. (2000). Structure and function of Cdc6/Cdc18: implications for origin recognition and checkpoint control. Mol. Cell *6*, 637–648.
26. Yamada, K., Kunishima, N., Mayanagi, K., Ohnishi, T., Nishino, T., Iwasaki, H., Shinagawa, H., and Morikawa, K. (2001). Crystal structure of the Holliday junction migration motor protein RuvB from *Thermus thermophilus* HB8. Proc. Natl. Acad. Sci. USA *98*, 1442–1447.
27. Putnam, C.D., Clancy, S.B., Tsuruta, H., Gonzalez, S., Wetmur, J.G., and Tainer, J.A. (2001). Structure and mechanism of the RuvB Holliday junction branch migration motor. J. Mol. Biol. *311*, 297–310.
28. Oyama, T., Ishini, Y., Cann, I.K.O., Ishino, S., and Morikawa, K. (2001). Atomic structure of the clamp loader small subunit from *Pyrococcus furiosus*. Mol. Cell *8*, 455–463.
29. Guenther, B., Onrust, R., Sali, A., O'Donnell, M., and Kuriyan, J. (1997). Crystal structure of the δ′ subunit of the clamp-loader complex of *E. coli* DNA polymerase III. Cell *91*, 335–345.
30. Jeruzalmi, D., Yurieva, O., Zhao, Y., Young, M., Stewart, J., Hingorani, M., O'Donnell, M., and Kuriyan, J. (2001). Mechanism of processivity clamp opening by the delta subunit wrench of the clamp loader complex of *E. coli* DNA polymerase III. Cell *106*, 417–428.

31. Jeruzalmi, D., O'Donnell, M., and Kuriyan, J. (2001). Crystal structure of the processivity clamp loader gamma (γ) complex of the *E. coli* DNA polymerase III. Cell *106*, 429–441.

32. Fodje, M.N., Hansson, A., Hannsson, M., Olsen, J.G., Gough, S., Willows, R.D., and Al-Karadghi, S. (2001). Interplay between an AAA module and an integrin I domain may regulate the function of magnesium chelatase. J. Mol. Biol. *311*, 111–122.

33. Holm, L., and Sander, C. (1996). Alignment of three-dimensional protein structures: network server for database searching. Methods Enzymol. *266*, 653–662.

34. Fahrner, R.L., Cascio, D., Lake, J.A., and Slesarev, A. (2001). An ancestral nuclear protein assembly: crystal structure of the *Methanopyrus kandleri* histone. Protein Sci. *10*, 2002–2007.

35. Karata, K., Inagawa, T., Wilkinson, A.J., Tatsuta, T., and Ogura, T. (1999). Dissecting the role of a conserved motif (the second region of homology) in the AAA family of ATPases: site-directed mutagenesis of the ATP-dependent protease FtsH. J. Biol. Chem. *274*, 26225–26232.

36. Karata, K., Verma, C.S., Wilkinson, A.J., and Ogura, T. (2001). Probing the mechanism of ATP hydrolysis and substrate translocation in the AAA protease FtsH by modelling and mutagenesis. Mol. Microbiol. *39*, 890–903.

37. Akiyama, Y., and Ito, K. (2000). Roles of multimerization and membrane association in the proteolytic functions of FtsH (HflB). EMBO J. *19*, 3888–3895.

38. Singh, K.S., Rozycki, J., Ortega, J., Ishikawa, T., Lo, J., Steven, A.C., and Maurizi, M.R. (2001). Functional domains of the ClpA and ClpX molecular chaperones identified by limited proteolysis and deletion analysis. J. Biol. Chem. *276*, 29420–29429.

39. Smith, C.K., Baker, T.A., and Sauer, R.T. (1999). Lon and Clp family proteases and chaperones share homologous substrate-recognition domains. Proc. Natl. Acad. Sci. USA *96*, 6678–6682.

40. Kihara, A., Akiyama, Y., and Ito, K. (1999). Dislocation of membrane proteins in FtsH-mediated proteolysis. EMBO J. *18*, 2970–2981.

41. Otwinowski, Z., and Minor, W. (1997). Processing X-ray diffraction data collected in oscillation mode. Methods Enzymol. *276*, 307–326.

42. Terwilliger, T.C., and Berendzen, J. (1999). Automated structure solution for MIR and MAD. Acta Crystallogr. D Biol. Crystallogr. *55*, 849–861.

43. Otwinowski, Z. (1991). Maximum likelihood refinement of heavy atom parameters. In Daresbury Study Weekend Proceedings (Warrington, UK: SERC Daresbury Laboratory), pp. 80–85.

44. Cowtan, K. (1994). Dm: an automated procedure for phase improvement by density modification. Joint CCP4 and ESF-EACBM Newsletter on Protein Crystallography *31*, 34–38.

45. Perrakis, A., Sixma, T.K., Wilson, K.S., and Lamzin, V.S. (1997). Warp: improvement and extension of crystallographic phases by weighted averaging of multiple refined dummy atomic models. Acta Crystallogr. D Biol. Crystallogr. *53*, 448–455.

46. Murshudov, G.N., Vagin, A.A., and Dodson, E.J. (1997). Refinement of macromolecular structures by the maximum likelihood method. Acta Crystallogr. D Biol. Crystallogr. *53*, 240–255.

47. Winn, M.D., Isupov, M.N., and Murshudov, G.N. (2001). Use of TLS parameters to model anisotropic displacement in macromolecular refinement. Acta Crystallogr. D Biol. Crystallogr. *57*, 122–133.

48. CCP4 (Collaborative Computational Project Number 4) (1994). The CCP4 suite: programs for protein crystallography. Acta Crystallogr. D Biol. Crystallogr. *50*, 760–763.

49. Laskowski, R.A., MacArthur, M.W., Moss, D.M., and Thornton, J.M. (1993). PROCHECK—a program to check the stereochemical quality of protein structures. J. Appl. Crystallogr. *26*, 283–291.

50. Brooks, B.R., Bruccoleri, R.E., Olafson, B.D., States, D.J., Swaminathan, S., and Karplus, M. (1983). CHARMM—a program for macromolecular energy, minimizations and dynamics calculations. J. Comput. Chem. *4*, 187–217.

51. Brunger, A.T., and Karplus, M. (1988). Polar hydrogen positions in proteins—empirical placement and neutron-diffraction comparison. Proteins Struct. Funct. Genet. *4*, 148–156.

52. Brzozowski, A.M., Savage, H., Verma, C.S., Turkenberg, J.P., Lawson, D.M., Svendsen, A., and Patkar, S. (2000). Structural origins of the interfacial activation in Thermomyces (Humicola) lanuginose lipase. Biochemistry *39*, 15071–15082.

53. Kraulis, P.J. (1991). MOLSCRIPT: a program to produce both detailed and schematic plots of protein structure. J. Appl. Crystallogr. *24*, 946–950.

54. Nicholls, A., Sharp, K.A., and Honig, B. (1991). Protein folding and association: insights from the interfacial and thermodynamic properties of hydrocarbons. Proteins Struct. Funct. Genet. *11*, 281–296.

Accession Numbers